Obstacle Avoidance of Flapping-Wing Air Vehicles Based on Optical Flow and Fuzzy Control

FU Qiang[1,2], *WANG Jin*[1], *GONG Le*[1], *WANG Jingyuan*[2], *HE Wei*[1,2*]

1. School of Automation and Electrical Engineering, University of Science and Technology Beijing, Beijing 100083, P.R. China;

2. Institute of Artificial Intelligence, University of Science and Technology Beijing, Beijing 100083, P.R. China

(Received 28 December 2020; revised 13 April 2021; accepted 20 April 2021)

Abstract: The flapping-wing air vehicle (FWAV) is a kind of bio-inspired robot whose wings can flap up and down like bird and insect wings. A vision-based obstacle avoidance method for FWAVs is proposed in this paper. First, the Farneback algorithm is used to calculate the optical flow field of the first-view video frames taken by the on-board image transmission camera. Based on the optical flow information, a fuzzy obstacle avoidance controller is then designed to generate the FWAV steering commands. Experimental results show that the proposed obstacle avoidance method can accurately identify obstacles and achieve obstacle avoidance for FWAVs.

Key words: dense optical flow; monocular vision; obstacle avoidance; flapping-wing air vehicle; fuzzy control

CLC number: TP242.6 **Document code:** A **Article ID:** 1005-1120(2021)02-0206-10

0 Introduction

The flapping-wing air vehicle (FWAV), involving bionics, aerodynamic analysis, mechanical structure analysis, energy, communication, control and other multidisciplinary technologies, is a new type of unmanned aerial vehicle that mimics the flight mode of birds or insects[1] to achieve flight[2-3]. The strengths of FWAVs are small size, high flight efficiency, low noise and strong flight maneuverability[4]. Therefore, FWAVs are promising to be used in military reconnaissance, field exploration, natural disaster rescue and other fields.

Obstacle avoidance is one of the indispensable capabilities for autonomous flight[5-7]. A FWAV has quite limited load capabilities, so common sensors such as laser rangers and radars are not suitable. With the advantages of light weight, low power consumption and rich information, vision sensors have proved to be a good choice for obstacle avoidance of FWAVs[8]. However, designing a practical obstacle avoidance system for FWAVs is still a problem to be solved.

One way of achieving obstacle avoidance is to use stereo vision. For example, the DelFly II[9] of the Delft University of Technology in The Netherlands contains an on-board stereo vision system which has two CMOS cameras running simultaneously at 30 Hz. DelFly II successfully avoids the walls of the indoor office space many times during the 72 s flight test. The experiment clearly demonstrates the potential of stereo vision for autonomous obstacle avoidance of FWAVs. The defections of DelFly II include short flight time and poor imaging quality of the visual perception system, so it cannot be used for more complex tasks.

The optical flow method, inspired from insects[10], is also an effective navigation means of FWAVs. Researchers adopt spherical cameras to obtain translational optical flow, and use it as the input of hovering flight and vertical landing control of an vertical take-off and landing unmanned aerial vehicle[11]. Edge-FS is a vision algorithm to determine velocity and depth[12]. A FWAV with an embedded

*Corresponding author, E-mail address: weihe@ieee.org.

How to cite this article: FU Qiang, WANG Jin, GONG Le, et al. Obstacle avoidance of flapping-wing air vehicles based on optical flow and fuzzy control[J]. Transactions of Nanjing University of Aeronautics and Astronautics, 2021, 38(2): 206-215.

http://dx.doi.org/10.16356/j.1005-1120.2021.02.002

STM32F4 is used as the experimental platform and the feasibility of Edge-FS is demonstrated on this platform. Optical flow is utilized to measure altitude for feedback control of a flapping-wing microrobot of 101 mg[13]. Ryu et al. from Seoul National University designed a FWAV with first-person view module and proposed an algorithm based on the time-to-contact (TTC). TTC was calculated from the optical flow[14-15]. Experiments demonstrated that the proposed algorithm could realize simple target tracking and obstacle avoidance.

Fuzzy control technology based on fuzzy theory is an advanced technology in modern industrial automation control[16-18]. It simulates human approximate reasoning as well as decision-making process, and is a fuzzy set control theory based on control language rules and fuzzy reasoning[19-20]. The complex structure of the FWAV makes it difficult to establish an accurate mathematical model, so a fuzzy control method is suitable for controlling FWAVs.

The main contributions of this paper are as follows: (1) Designing an obstacle avoidance method for FWAVs based on dense optical flow and fuzzy control; (2) implementing real experiments to verify the effectiveness of the proposed obstacle avoidance method.

The structure of this paper is organized as follows. Section 1 introduces the principle and calculation process of Farneback optical flow, as well as the principle of fuzzy control and the design process of the fuzzy controller. Section 2 describes the parameters of the FWAV, image transmission camera and flight control module. In Section 3, the control system of the FWAV is tested and the obstacle avoidance experiment results are presented. Section 4 draws the conclusions and extends future work.

1 Algorithm for Obstacle Avoidance

1.1 Optical flow

1.1.1 Farneback dense optical flow

Optical flow is the instantaneous velocity of the pixel movement of a space moving object on the image plane[21]. It was put forward by Gibson in The Perception of the Visual World[22] in 1952. There are two basic assumptions: (1) When a target moves between different frames, its brightness will not change; (2) The pixel displacement between adjacent frames ought to be small. Then the basic constraint equation of optical flow can be obtained[23]

$$I(x,y,t)=I(x+\mathrm{d}x,y+\mathrm{d}y,t+\mathrm{d}t) \tag{1}$$

where $I(x,y,t)$ means the intensity of pixel point (x,y) in the image plane at time t and $\mathrm{d}x$; $\mathrm{d}y$ the small displacements of pixel between the frame at time t and $t+\mathrm{d}t$ in x-axis and y-axis, respectively.

From Eq.(1) we can get

$$I_x u+I_y v+I_t=0 \tag{2}$$

where $I_x=\dfrac{\partial I}{\partial x}, I_y=\dfrac{\partial I}{\partial y}, I_t=\dfrac{\partial I}{\partial t}$ can be obtained from image data and $u=\dfrac{\mathrm{d}x}{\mathrm{d}t}, v=\dfrac{\mathrm{d}y}{\mathrm{d}t}$ are the optical flow vector to be calculated.

There is only one constraint equation, and there are two unknown variables in Eq.(2), so we cannot directly calculate the optical flow vector. In the literatures, there are many methods to calculate the optical flow[24-26]. This paper computes the optical flow by the method proposed by Farneback[27].

Unlike the traditional sparse optical flow methods that only calculate the optical flow of feature points, the Farneback method, a dense optical flow methods computes the optical flow of all pixels on the image. The sparse optical flow methods, like the pyramid L-K method, sometimes fail to detect the corners of obstacles so that the FWAV fails to avoid obstacles. The pyramid L-K method is compared with the Farneback method. The result of the pyramid L-K method is shown in Fig.1, the trunk is not detected and the result of the Farneback method is shown in Fig.2.

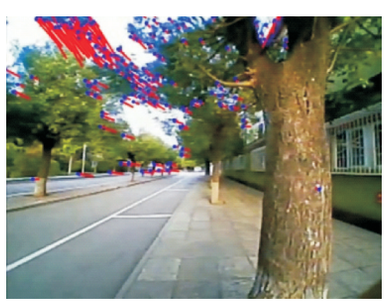

Fig.1 Results of the pyramid L-K method detection of obstacles

Fig.2 Results of the Farneback method detection of obstacles

1.1.2 Obstacle detection

When the FWAV moves forward, the camera transmits images to the ground station. Each image is divided into the left and the right parts, and the obstacle avoidance system calculates the optical flow field of the left and the right parts, seperately.

The flight of the FWAV will not be affected by obstacles on the edge of the image, so we only need to calculate the optical flow in the central area of each image, and compute the normalisation of the difference of optical flow values between the left and the right fields[28]

$$e = F_{\mathrm{L}} - F_{\mathrm{R}} = \frac{\sum \| W_{\mathrm{L}} \| - \sum \| W_{\mathrm{R}} \|}{\sum \| W_{\mathrm{L}} \| + \sum \| W_{\mathrm{R}} \|} \tag{3}$$

where $F_{\mathrm{L}}, F_{\mathrm{R}}$ are the average vector moduli; $W_{\mathrm{L}}, W_{\mathrm{R}}$ the sums of optical flow vector moduli, and the subscript L, R indicate that the variable is the value of the left or the right optical flow field. There is no obstacle when $\sum \| W_{\mathrm{L}} \| + \sum \| W_{\mathrm{R}} \|$ is very small. Therefore, if $\sum \| W_{\mathrm{L}} \| - \sum \| W_{\mathrm{R}} \| \neq 0$, e will be very large, so e is set to 0 when $\sum \| W_{\mathrm{L}} \| + \sum \| W_{\mathrm{R}} \| < \varepsilon$ (ε is a threshold value).

If $e > 0$, the FWAV needs to turn right; if $e < 0$, the FWAV needs to turn left; if $e = 0$, the FWAV keeps going straight. Therefore, the difference value e in Eq.(3) is set to the input of the fuzzy controller.

1.2 Fuzzy control

1.2.1 Theory of fuzzy control

The fuzzy control process is divided into three steps: Fuzzification, fuzzy logic inference and defuzzification judgment[29]. It is completed by the fuzzifier, fuzzy inference engine and defuzzifier[30]. The structure of a fuzzy controller is shown in Fig.3.

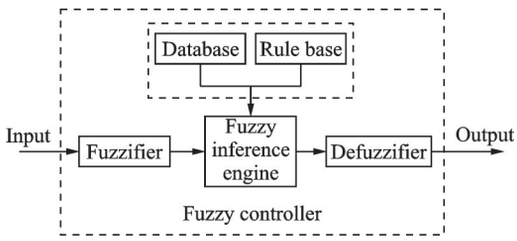

Fig.3 Structure of a fuzzy controller

1.2.2 Fuzzy controller design

The fuzzy controller designed in this paper has two inputs and one output, where the inputs are e in Eq.(3) and its derivative term $\dot{e}$, and the output is the FWAV control signal u. The symbol of u represents the turning direction of the FWAV, and the amplitude of u represents the turning amplitude.

The fuzzy subsets of $e, \dot{e}, u$ are [NB, NM, NS, ZO, PS, PM, PB], and the quantificational field domain is $[-3, -2, -1, 0, 1, 2, 3]$. Note that "N" means the output $u<0$, and the FWAV will turn left; "ZO" means the output $u=0$, and the FWAV will go straight; "P" means the output $u>0$, and the FWAV will turn right; "S" "M" and "B" represent the outputs, that is, the steering amplitudes of the FWAV. In order to obtain the corresponding fuzzy subset of $e, \dot{e}, u$, they must be converted to the interval $[-3, 3]$. The transformation equations are described as follows

$$e_1 = K_e e \left(K_e = \frac{3}{e_{\max}} \right) \tag{4}$$

$$\dot{e}_1 = K_{\dot{e}} \dot{e} \left(K_{\dot{e}} = \frac{3}{\dot{e}_{\max}} \right) \tag{5}$$

$$u = \frac{u_1}{K_u} \left(K_u = \frac{3}{u_{\max}} \right) \tag{6}$$

where $e_1, \dot{e}_1, u_1$ are the corresponding values in the interval $[-3, 3]$, and $e_{\max} = 1, \dot{e}_{\max} = 10, u_{\max} = 1$ are determined by the experiment. In order to prevent the phenomenon of spikes caused by disturbances, a saturation module is added in the calculation.

If $e_1, \dot{e}_1, u_1$ are between fuzzy subset A and fuzzy subset B, the corresponding fuzzy subset value is $\mu_A A + \mu_B B$, where μ_A and μ_B are memberships of fuzzy subset A and fuzzy subset B(the values of μ_A and μ_B are determined by the membership function). If the fuzzy subset is represented by a matrix, for example, $e_1 = \mu_A \mathrm{NB} + \mu_B \mathrm{NM}$, it can be represented by a 1×7 matrix $\boldsymbol{M}_{e_1} = [\mu_A, \mu_B, 0, 0,$

0, 0, 0]. As shown in Fig.4, the membership functions are all triangular membership functions.

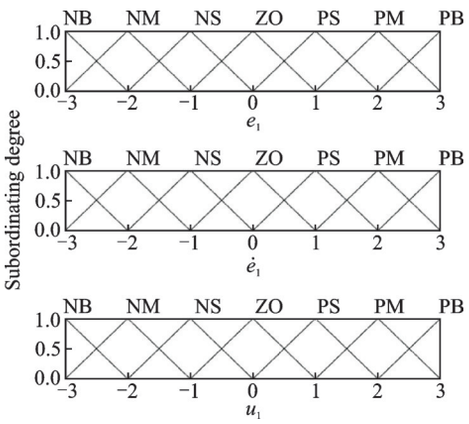

Fig.4 Membership functions

After obtaining the fuzzy subsets of e_1 and $\dot{e}_1$, the fuzzy subset of u_1 can be obtained through the fuzzy rule table which is derived from experiences. The rule-table of fuzzy inference system (FIS) about u_1 in this paper is as follows.

In Table 1, "N" means that if the output <0, the FWAV will turn left; "P" means that if the output $u>0$, and the FWAV will turn right. "S", "M" and "B" represent the outputs, that is, the steering amplitudes of the FWAV.

The fuzzy operation relationships that are formed by 49 conditional statements can be obtained from Table 1. The calculation process of one conditional statement "if e_1, $\dot{e}_1$, then $\boldsymbol{u}_1$" is as follows.

Table 1 Rule-table of FIS about u_1

u_1		e_1						
		NB	NM	NS	ZO	PS	PM	PB
e_1	NB	PB	PB	PM	PS	NS	NS	NM
	NM	PB	PB	PS	PS	NM	NS	NM
	NS	PB	PM	PS	PS	NM	NM	NB
	ZO	PB	PM	PS	ZO	NM	NM	NB
	PS	PB	PM	PS	NS	NM	NM	NB
	PM	PM	PS	PS	PN	NM	NM	NB
	PB	PM	PS	PS	NS	NM	NB	NB

Step 1 Calculate the 7×7 matrix $\boldsymbol{D}_1$

$$\boldsymbol{D}_1=\boldsymbol{M}_{e_1}^{\mathrm{T}}\times\boldsymbol{M}_{\dot{e}_1}=\begin{bmatrix} d_{11} & \cdots & d_{17} \\ \vdots & \ddots & \vdots \\ d_{71} & \cdots & d_{77} \end{bmatrix}$$

where $\boldsymbol{M}_{e_1}$, $\boldsymbol{M}_{\dot{e}_1}$ are the matrices of the fuzzy subset of e_1 and $\dot{e}_1$.

Step 2 Transform matrix $\boldsymbol{D}_1$ into 49-dimensional column vector $\boldsymbol{D}_{T1}$

$$\boldsymbol{D}_{T1}=[\,d_{11},\cdots,d_{17},d_{21},\cdots,d_{27},\cdots,d_{77}\,]^{\mathrm{T}}$$

Step 3 Calculate the 49×7 fuzzy relationship matrix $\boldsymbol{R}_1$

$$\boldsymbol{R}_1=\boldsymbol{D}_{T1}\times\boldsymbol{u}_1$$

After finding the matrices corresponding to all 49 conditional sentences, take the union of the matrices (take the larger element of them) and finally get the fuzzy relationship matrix $\boldsymbol{R}$.

Based on $\boldsymbol{D}_{T1}$ and $\boldsymbol{R}$, the matrix of $\boldsymbol{u}_1$ can be calculated by $\boldsymbol{u}_1=\boldsymbol{D}_{T1}\times\boldsymbol{R}$. Therefore, we can get the fuzzy subset of $\boldsymbol{u}_1$.

After obtaining the fuzzy subset of $\boldsymbol{u}_1$, it must be defuzzified and divided by K_u to obtain the true output value of the fuzzy controller. If the fuzzy subset of u is composed by fuzzy subset X_1 and fuzzy subset X_2, the value of u_1 can be defuzzified by

$$\boldsymbol{u}_1=\mu_{X_1}x_1+\mu_{X_2}x_2 \tag{7}$$

where x_1, x_2 are the corresponding values of the fuzzy subsets X_1 and X_2, respectively, when the membership degree is 1; μ_{X_1} and μ_{X_2} the memberships of fuzzy subset X_1 and fuzzy subset X_2, respectively. The controller output u can be calculated by Eq.(6).

The entire control system is a closed loop as shown in Fig.5.

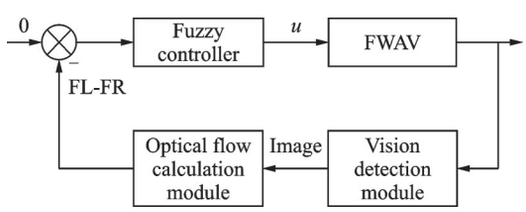

Fig.5 Diagram of control system block diagram

2 Hardware Preparation

2.1 FWAV platform

As shown in Fig.6, the FWAV adopts an X-wing structure with two pairs of wings. The FWAV weighs 18 g and has a wingspan of 27 cm. The fuselage is very light because it is made from hard plastic, and the wings are made from polyvinyl chloride. The flight of the FWAV is driven by a 6 mm hollow cup motor with a speed of 4 200 r/min, and the transmission ratio is 1∶25.4. The power supply is

provided by a 3.7V-70 mA·h lithium battery. The flight speed of the FWAV is about 5 m/s, and the wing flapping frequency is 16 Hz. Due to its light body weight and small wing area, the FWAV has weak wind resistance and can only fly indoors or outdoors in windless weather.

Fig.6 FWAV platform

As shown in Fig.7, the FWAV is equipped with a video transmission camera module to transmit images to the ground station. The camera weighs 4.6 g, the size of the captured image is 640 pixel × 480 pixel, and the FOV is 45°. It communicates with the ground station through 5.8 GHz wireless signal.

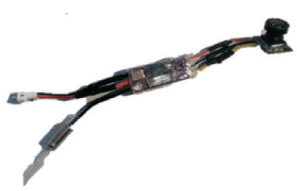

(a) Video transmission camera and antenna

(b) Receiver used with the ground station

Fig.7 Camera data transmission module

The ground station is a laptop, whose configuration is shown in Table 2.

Table 2 Configuration of the ground station

Property	Value
Operating system	Windows 10
CPU	i5-9400HF
GPU	GTX-1660ti
RAM/GB	16

The ground station software is written by C++ based on the Qt5 platform. The image processing part is based on the OpenCV open-source function library. The main interface of the ground station software is shown in Fig.8.

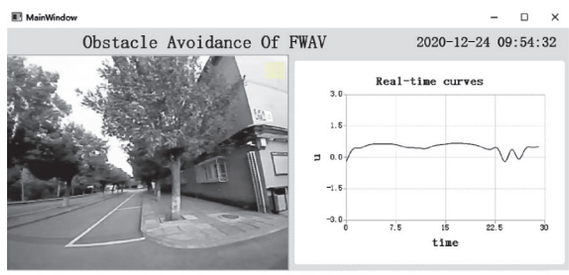

(a) The original image (b) Value of controller output

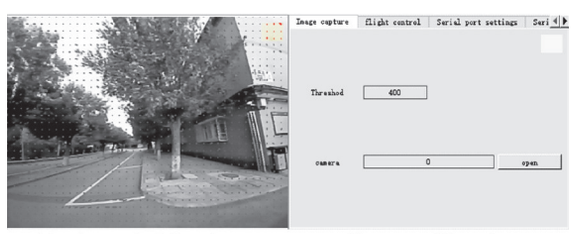

(c) The optical flow image (d) Control interface

Fig.8 Main interface of the ground station software

2.2 Flight control module

Flight control is realized by a self-developed flight control module, which is shown in Fig.9. The parameters are as follows: Length 20.45 mm, width 15.74 mm, weight 6.24 g. The flight control module contains a 32-bit low-power chip STM32F103C8T6 based on ARM Cortex-M3 architecture, voltage regulator module xc6206, two 5 V servo output ports, and a 5 V communication interface. The circuit board uses 5 V power supply. During the flight, the FWAV sends image information to the ground station through the camera data transmission module, and the ground station sends control commands to the data transmission module to control the steering of the FWAV.

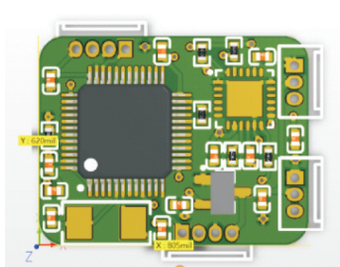

Fig.9 Flight control module

The ground station sends the control signal to the FWAV through HC-12 wireless serial communication module, as shown in Fig.10. The whole experiment system of obstacle avoidance is shown in Fig.11.

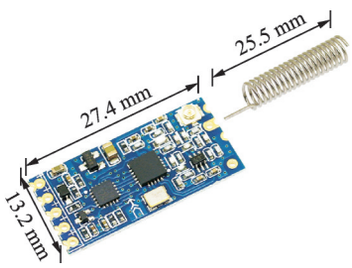

Fig.10 HC-12 wireless serial communication module

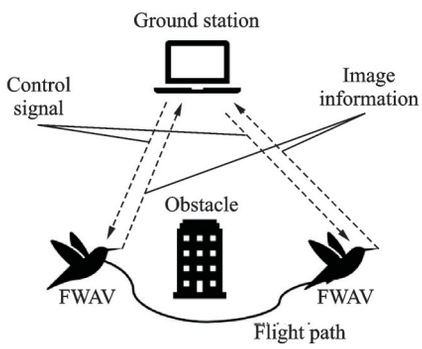

Fig.11 Experiment system

3 Experimental Results

3.1 Control system test

Before conducting the FWAV obstacle avoidance experiment, a video is taken with a camera in hand, which is used as an input to the controller to test whether the controller's output has the desired effect.

The parameters of the fuzzy controller are as follows: $e_{max}=1$, $\dot{e}_{max}=10$, $u_{max}=1$, $K_e=3$, $K_{\dot{e}}=0.3$, $K_u=3$ and the threshold $\varepsilon=400$, which is determined by the flight experiments in a background monotonic environment.

As shown in Fig.12, we use a tree as an obstacle and walk towards it from far to near and record F_L, F_R. The controller outputs results during the process, as shown in Fig.13.

At 3—5 s the obstacle is close and in the right half of the field, thus the controller output u is negative. The video is taken by a person walking with a hand-held camera, so the optical flow vector is small, and the fuzzy subset of u is almost NS.

However, the output has unexpected glitch at $u>0$, since the selected background color is not monotonous. To solve the problem, we filter the output

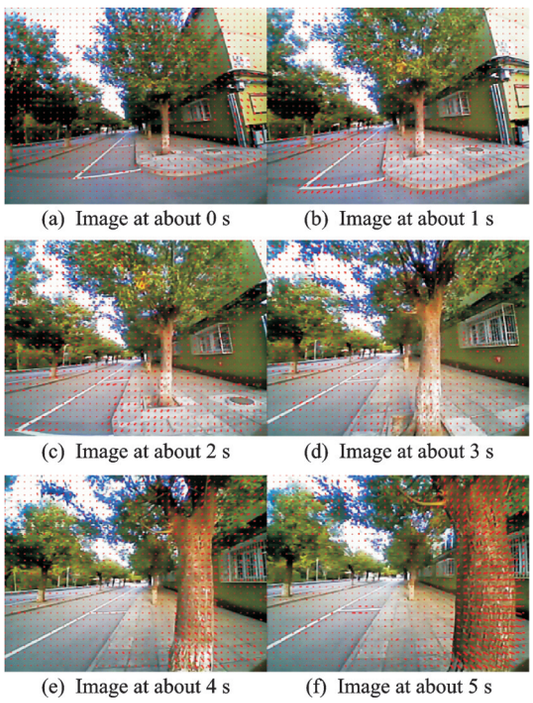

(a) Image at about 0 s (b) Image at about 1 s

(c) Image at about 2 s (d) Image at about 3 s

(e) Image at about 4 s (f) Image at about 5 s

Fig.12 Recorded sequential images (testing)

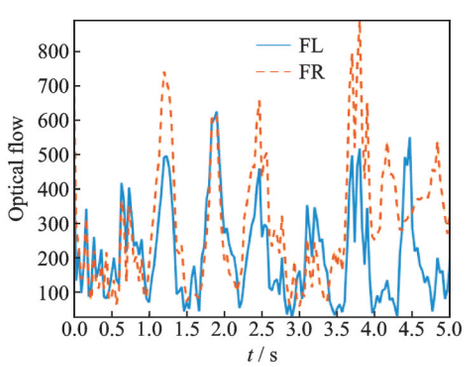

(a) Optical flow values for the left and right field of view

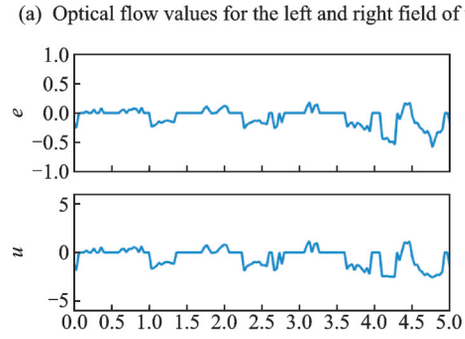

(b) Differential optical flow values and controller output signals

Fig.13 Experimental data (testing)

signal u, calculate the average value of it every five frames and output every five frames, as shown in Fig.14.

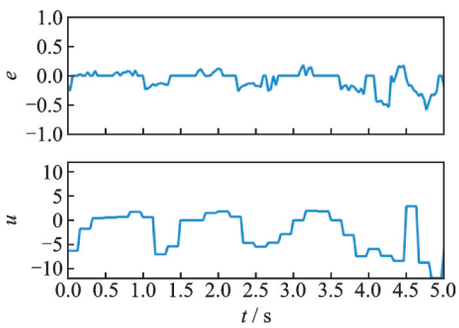

Fig.14 Control signal output every five frames

3.2 Experimental results

In the experiments, two boxes are used as obstacles for the FWAV and the obstacles are shown in Fig.15. We conduct two experiments to verify whether the FWAV can successfully avoid obstacles in different situations.

During the first obstacle avoidance experiment, the distance between the two obstacles is set to 1.0 m. When the FWAV turn left to avoid the first obstacle, the second obstacle is at the right side of the FWAV, causing the FWAV to continue to turn left. The first flight path of the FWAV is shown in Fig.16. The recorded images are shown in Fig. 17 and the data of experiment is shown in Fig.18.

Fig.15 The obstacles

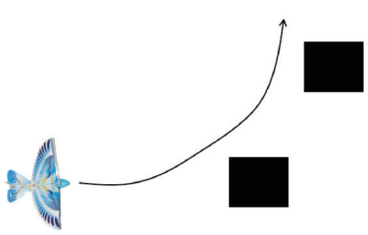

Fig.16 The first flight path of the FWAV

(a) Image at about 0 s (b) Image at about 0.2 s

(c) Image at about 0.8 s (d) Image at about 1.3 s

(e) Image at about 1.6 s (f) Image at about 2 s

Fig.17 The recorded images of the first flight

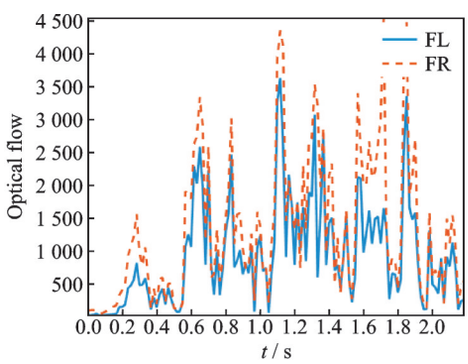

(a) Optical flow values for the left and right field of view

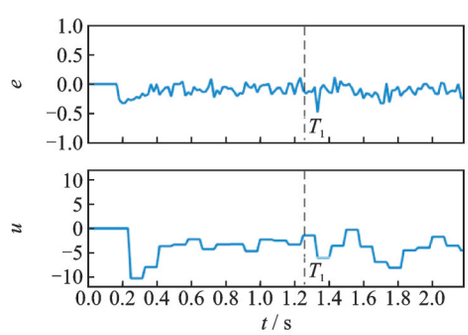

(b) Differential optical flow values and controller output signals

Fig.18 The data of the first flight

Since the obstacles always appear in the right half of the FWAV, $F_L < F_R$ and $u < 0$. The FWAV avoids the first obstacle before time T_1, and the difference e is large during the periods 0.2—0.4 s and 1.6—1.8 s because the FWAV is close to the obstacles.

During the second obstacle avoidance experi-

ment, the distance between the two obstacles is set to 1.5 m. When the FWAV turns left to avoid the first obstacle, the second obstacle is at the left of the FWAV, causing the vehicle to turn right. The second flight path of the FWAV is shown in Fig.19, the recorded images are shown in Fig.20 and the data of experiment is shown in Fig.21.

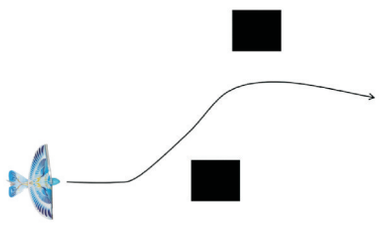

Fig.19 The second flight path of the FWAV

(a) Image at about 0.5 s (b) Image at about 1 s

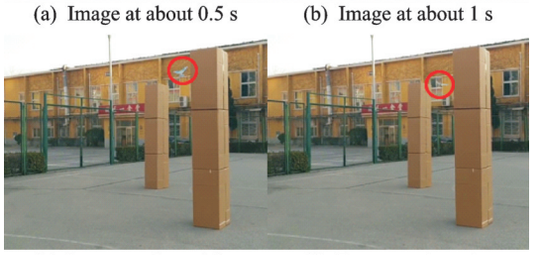

(c) Image at about 1.2 s (d) Image at about 2 s

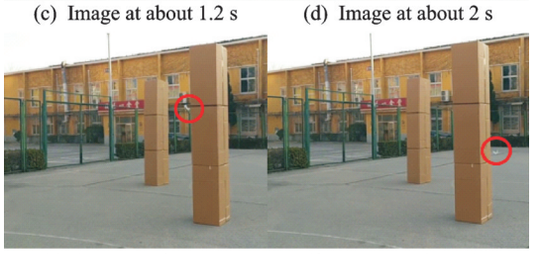

(e) Image at about 3 s (f) Image at about 4 s

Fig.20 The recorded images of the second flight

Before time T_2, $F_L < F_R$ and $u < 0$, so the FWAV turns left to avoid the first obstacle. After time T_2, $F_L > F_R$ and $u > 0$, then the FWAV turns right to avoid the second obstacle. The difference e is large during the periods 1.2—1.4 s and 2.4—2.6 s because the FWAV is very close to the obstacles. During 2.7—2.9 s the output u is unreasonably less than 0, which is due to the complex background. During 3—3.7 s, the FWAV has avoided obstacles, but the output u is still large because there is a basketball hoop which is incorrectly considered as an obstacle by the obstacle avoidance system.

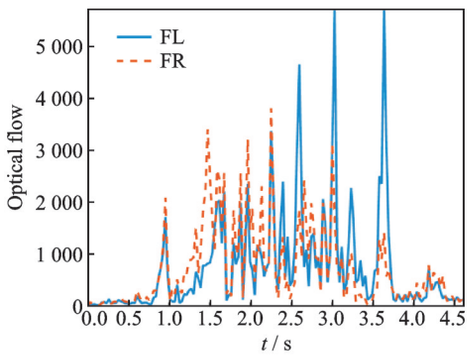

(a) Optical flow values for the left and right field of view

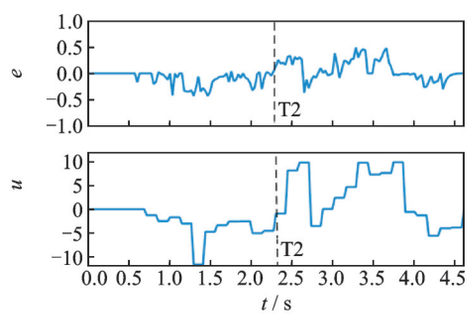

(b) Differential optical flow values and controller output signals

Fig.21 The data of the second flight

The above two experiments show that the steering of the FWAV is not affected by wind and load capacity, and the proposed obstacle avoidance method is feasible and effective. However, the controller may be susceptible to the influence of the complex environment.

4 Conclusions

In this paper, aiming at the obstacle avoidance problem of FWAV, a vision-based obstacle avoidance method is proposed based on the Farneback optical flow algorithm and fuzzy control. In addition, an X-wing aerial vehicle is modified as the experimental platform for experiments. Experimental results demonstrate the effectiveness of the proposed obstacle avoidance method. The proposed method does not require complex mathematical modelling of the FWAV and is simple as well as easy to implement. In future work, we will add effective filters to the control system to make it achieve better performance under complex backgrounds, and use neural

network to train the controller parameters to achieve more precise control.

References

[1] WOOD R J. The first takeoff of a biologically inspired at-scale robotic insect[J]. IEEE Transactions on Robotics, 2008, 24(2): 341-347.

[2] HE W, DING S Q, SUN C Y. Research progress on modeling and control of flapping-wing air vehicles[J]. Acta Automatica Sinica, 2017, 43(5): 685-696.

[3] HE W, MU X X, ZHANG L, et al. Modeling and trajectory tracking control for flapping-wing micro aerial vehicles[J]. IEEE/CAA Journal of Automatica Sinica, 2021, 8(1): 148-156.

[4] YIN Z, HE W, ZOU Y, et al. Efficient formation of flapping-wing aerial vehicles based on wild geese queue effect[J]. Acta Automatica Sinica, 2020, 46: 1-13.

[5] FU Q, YANG Y H, CHEN X Y, et al. Vision-based obstacle avoidance for flapping-wing aerial vehicles[J]. Science China Information Sciences, 2020, 63(7): 170208.

[6] CHEN M, TAO G. Adaptive fault-tolerant control of uncertain nonlinear large-scale systems with unknown dead zone[J]. IEEE Transactions on Cybernetics, 2016, 46(8): 1851-1862.

[7] REN Y, CHEN M, LIU J Y. Bilateral coordinate boundary adaptive control for a helicopter lifting system with backlash-like hysteresis[J]. Science China Information Sciences, 2020, 63(1): 119203.

[8] FU Q, CHEN X Y, ZHENG Z L, et al. Research progress on visual perception system of bionic flapping-wing aerial vehicles[J]. Journal of Engineering Sciences, 2019, 41(12): 15-22.

[9] ROON G C H E D, PERIN M, REMES B D W, et al. The DelFly: Design, aerodynamics, and artificial intelligence of a flapping wing robot[M]. Germany: Springer Publishing Company, Incorporated, 2015.

[10] RINIVASAN M V, ZHANG S W, CHAHL J S, et al. How honeybees make grazing landings on flat surfaces[J]. Biological Cybernetics, 2000, 83(3): 171-183.

[11] ERISSE B, USSOTTO F X, HAMEL T, et al. Hovering flight and vertical landing control of a VTOL unmanned serial vehicle using optical flow[C]//Proceedings of IEEE/RSJ International Conference on Intelligent Robots & Systems.[S.l.]: IEEE, 2008:1-11.

[12] IMBERLY M, CROON G D, WAGTER C D, et al. Efficient optical flow and stereo vision for velocity estimation and obstacle avoidance on an autonomous pocket drone[J]. IEEE Robotics and Automation Letters, 2017, 2(2): 1070-1076.

[13] DUHAMEL P E J, PEREZ-ARANCIBIA N O, BARROWS G L, et al. Biologically inspired optical-flow sensing for altitude control of flapping-wing microrobots[J]. IEEE/ASME Transactions on Mechatronics, 2013, 18(2): 556-568.

[14] RYU S, LEE J, KIM H J. Optical flow on a flapping wing-micro air vehicle to avoid collisions and steer[C]//Proceedings of the 30th Congress of the International Council of The Aeronautical Sciences (ICAS). Daejeon, Korea: ICAS, 2016:1-6.

[15] RYU S, KWON U, KIM H J. Autonomous flight and vision-based target tracking for a flapping-wing MAV[C]//Proceedings of IEEE/RSJ International Conference on Intelligent Robots and Systems (IROS). Daejeon, Korea: IEEE, 2016: 5645-5650.

[16] LIU Y M, WANG W, WANG X D, et al. A fuzzy control strategy combined wind power prediction and energy storage SOE for smooth wind power output[J]. Power System Technology, 2019, 43(7): 2535-2543.

[17] CHEN M, SHAO S Y, JIANG B. Adaptive neural control of uncertain nonlinear systems using disturbance observer[J]. IEEE Transactions on Cybernetics, 2017, 47(10): 3110-3123.

[18] ZHU B, ZHU J Z, CHEN Q W. A bio-inspired flight control strategy for a tail-sitter unmanned aerial vehicle[J]. Science China Information Sciences, 2020, 63(7): 170203.

[19] MACVICAR-WHELAN P J. Fuzzy sets for man-machine interaction[J]. International Journal of Man Machine Studies, 1976, 8(6): 687-697.

[20] XIE G, SHANGGUAN A Q, FEI R, et al. Motion trajectory prediction based on a CNN-LSTM sequential model[J]. Science China Information Sciences, 2020, 63(11): 212207.

[21] EGELHAAF M, KERN R. Vision in flying insects[J]. Current Opinion in Neurobiology, 2003, 12(6): 699-706.

[22] ARNHEIM R, GIBSON J J. The perception of the visual world[J]. Journal of Aesthetics & Art Criticism, 1952, 11(2): 172-173.

[23] WANG F, CUI J Q, CHEN B M, et al. A comprehensive UAV indoor navigation system based on vision optical flow and laser FastSLAM[J]. Acta Automatica Sinica, 2013, 39(11): 1889-1900.

[24] POGGIO T, REICHARDT W. Nonlinear interactions underlying visual orientation behavior of the

fly[J]. Cold Spring Harbor Symposia on Quantitative Biology, 1976, 40: 635-645.
[25] HORN B K P, SCHUNCK B G. Determining optical flow[J]. Artificial Intelligence, 1980, 17(1/2/3): 185-203.
[26] LUCAS B D, KANADE T. An iterative image registration technique with an application to stereo vision[C]//Proceedings of the 7th International Joint Conference on Artificial Intelligence (IJCAI'81).[S.l.]: ACM, 1981: 674-679.
[27] FARNEBACK G. Two-frame motion estimation based on polynomial expansion[C]//Proceedings of the 13th Scandinavian Conference on Image Analysis (SCIA 2003). Berlin, Germany: Springer, 2003: 363-370.
[28] XIAO X, CHEN Y H. Autonomous mobile robot obstacle avoidance system based on optical flow[J]. Computer Engineering, 2013, 39(10): 305-308.
[29] NAN Y, CHEN H X, YANG Y, et al. Primary methodologies of modern control: Status and prospect[J]. Journal of Nanjing University of Aeronautics & Astronautics, 2015, 47(6): 798-810.(in Chinese)
[30] GONZALEZA J, GOMARIZA S, BATLLEB C, et al. Fuzzy controller for the yaw and velocity control of the Guanay II AUV[J]. IFAC-PapersOnLine, 2015, 48(2): 268-273.

Acknowledgements This work was supported in part by the National Natural Science Foundation of China (Nos. 61803025, 62073031), the Interdisciplinary Research Project for Young Teachers of USTB (Fundamental Research Funds for the Central Universities) (No. FRF-IDRY-19-010), and the Beijing Top Discipline for Artificial Intelligent Science and Engineering, University of Science and Technology Beijing.

Authors Dr. **FU Qiang** received the B.E. degree in thermal energy and power engineering from Beijing Jiaotong University, China in 2009, and the Ph.D. degree in control science and engineering from Beihang University (formerly Beijing University of Aeronautics and Astronautics), China in 2016. He is currently an associate professor in the School of Automation and Electrical Engineering, University of Science and Technology Beijing, China. His research interests include flapping-wing aerial vehicle, vision-based navigation and 3D vision.

Prof. **HE Wei** received the B.E. degree in automation and the M.E. degree in control science and engineering, both from College of Automation Science and Engineering, South China University of Technology (SCUT), China in 2006 and 2008, respectively, and the Ph.D. degree in control theory and control engineering from Department of Electrical & Computer Engineering, the National University of Singapore (NUS), Singapore in 2011. He is currently working as a full professor in School of Automation and Electrical Engineering, University of Science and Technology Beijing, China. His research interests include robotics, distributed parameter systems and intelligent control systems.

Author contributions Dr. **FU Qiang** guided this study and revised the manuscript. Mr. **WANG Jin** designed the study, wrote the code, analyzed the data and wrote the manuscript. Mr. **GONG Le** helped to modify the FWAV and conducted the experiment. Mr. **WANG Jingyuan** and Prof. **HE Wei** revised the manuscript. All authors commented on the manuscript draft and approved the submission.

Competing interests The authors declare no competing interests.

(Production Editor: ZHANG Bei)

基于光流法和模糊控制的扑翼飞行器避障研究

付 强[1,2], 王 进[1], 宫 乐[1], 王靖元[2], 贺 威[1,2]

(1.北京科技大学自动化学院,北京 100083,中国; 2.北京科技大学人工智能研究院,北京 100083,中国)

摘要: 扑翼飞行器是一种仿生机器人,其翅膀可以像鸟和昆虫的翅膀一样上下扑动。本文提出了一种基于视觉的扑翼飞行器避障方法。首先,使用稠密光流算法计算机载图像传输摄像机拍摄的第一视角视频帧的光流场。基于所获取光流信息作为输入量,设计模糊避障控制器来给出扑翼飞行器的导航指令。实验结果表明,本文所提出的避障方法能够准确识别障碍物,实现扑翼飞行器的避障。

关键词: 稠密光流;单目视觉;避障;扑翼飞行器;模糊控制